# Chapter 4

# Performance assessment of a passive solar still integrated with thermal energy storage and nanoparticle stored in copper cylinders

## 4.1 Overview

In the present study, nanoparticle (CuO) has been dispersed in paraffin wax and stored in a copper cylinder to enhance the thermal conductivity and increase the total daily production of the solar distillation unit. Experiments have been performed for comparison between simple solar still (SSS), solar still with phase change material (SSPCM), and solar still with phase change material doped with nanoparticle (SSNPCM). The mixing of nanoparticle causes a paradigm shift of the thermo-physical properties of phase change material (PCM). Nanoparticle and copper cylinder enhance the heat transfer rate with decreased duration of sensible heating, melting and solidification of PCM. Thermal analysis reveals that the evaporative mode of heat transfer has dominated heat transfer between glass cover and water. The maximum and average temperature for water basin and NPCM has been increased significantly for SSNPCM. The daily productivity of SSPCM and SSNPCM has been increased by 40.5 and 94.19 % as compared to SSS. Based on the heat transfer rate, thermal conductivity, and daily productivity, SSNPCM can be considered not only as a better performing system as compared to SSS and SSPCM but also as a low cost disruptive technology in resource-constrained settings where drinking water is really scarce.

## 4.2 Materials and methods

### 4.2.1 Experimental procedure

Fig.1 shows the schematic and detailed explanation for the experimental setup where passive solar still having a single slope (75 cm x 75 cm x 15 cm) has been fabricated from stainless steel (1 mm thickness). The solar still consists of a transparent covering which covers the water

basin and the water basin was colored with black colour acting as a basin liner. The cover is substantially transparent to solar radiation and opaque to infrared and serves as a condenser for the saturated vapor within the solar still. The radiation shape factor strongly depends on the solar still geometry especially the portion of the inclined glass cover with respect to the basin water at the horizontal level, although the distillation output varies very little with the variation of the inclination of the glass cover.

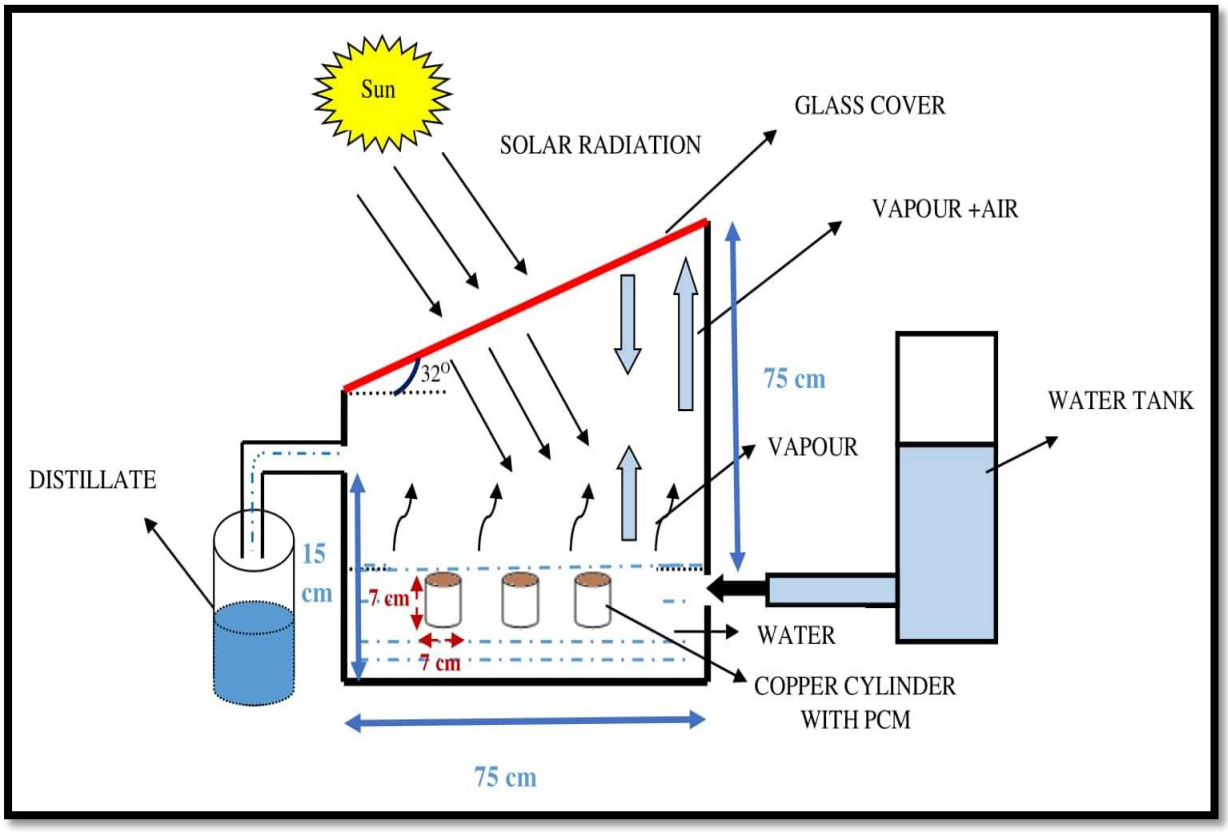


**Fig. 4.1** Schematic of the experimental set-up

**Fig. 4.2** A photographic view of the experimental setup


**Fig. 4.3** A photographic view of (a) copper cylinders, (b) copper cylinders with PCM, (c) paraffin wax, (d) nanoparticle (CuO), and (e) copper cylinder with nanoparticle doped in PCM

The solar still has been coupled with six cylinders loaded with PCM or NPCM, and cylinders have been made from copper sheet to raise the thermal conductivity. The dimension of the copper cylinder has been 7 cm diameter with 7 cm in height. All six copper cylinders, while filled with PCM or NPCM, have been sealed with rubber rings operational within the desired range of temperature in the present study. Experiments have been performed for simple solar still, solar still with PCM, and NPCM in order to compare the performance in terms of daily productivity and heat transfer. In the present study, the quantity of water in the basin has been kept around 39.2 kg for water level at 7 cm, whereas when the copper cylinder with PCM or NPCM have been used the quantity of water in the basin reduces to 37.6 kg with water level maintained at 7 cm.

**Table 4.1** Thermo-physical properties of paraffin wax (Farid et al., 2004; Sharma et al., 2009; Zalba et al., 2003)

| **Thermophysical properties** | **Paraffin wax** |
|---|---|
| **Chemical formula** | ( $C_{31}H_{64}$) |
| **Melting point ($^oC$)** | 58-60 $^oC$ |
| **Latent heat (fusion), kJ/kg** | 226 |
| **Density (solid), kg/m$^3$** | 818 |
| **Conductivity (thermal), W/m-K** | 0.25 |
| **Specific heat, kJ/kg-$^oC$** | 2.95 |

**Table 4.2** The used nanoparticle specifications

| Item | CuO specifications |
|---|---|
| **Manufacturer** | Sisco research laboratories pvt. Ltd. (28954) |
| **Assay** | Min. 99% |
| **Appearance** | Black powder |
| **PH value** | 7.5 |
| **Grain size (nm)** | 40 |
| **Thermal conductivity, W/m-K** | 0.34 |

The experiment has been conducted at the Indian Institute of Technology, Department of Mechanical Engineering, Banaras Hindu University, India, during October month starting from 09.00 AM and finishing at 08.00 PM, and the weather during the observation has been clear. The variables such as ambient and basin water temperature have been measured hourly until no further distillation has been observed, and heat transfer seizes. The temperature at different points has been recorded using P-T 100 thermometer.

**Table 4.3** Experimental variables

| Variables | Symbols | Value |
|---|---|---|
| **Transmittance (glass cover)** | $\tau_g$ | 90% |
| **absorptivity (glass cover)** | $\varepsilon_g$ | 5% |
| **Wind speed** | V | 1 m/s |
| **Density (water)** | $\rho$ | 989 kg/m$^3$ |
| **Latent heat of vaporization** | $h_{fg}$ | 2372 (KJ/kg) |
| **Declination angle** | $\delta$ | 32$^o$ |
| **Latitude of Varanasi** | $\varphi$ | 25.31$^o$ |

Tables 4.1 and 4.2 depicts the thermo physical properties of paraffin wax and CuO (nanoparticle). The experimental variables observed during the present study have been given in Table 4.3. An anemometer and a solar power meter with their range of operation and accuracy have been presented in Table 4.4 and have been used to compute the velocity of wind and incident solar radiation, respectively. Fig. 4.2 presented the photographic view of the experimental system and Fig. 4.3 depicts the copper cylinders used to store the PCM or NPCM doped with CuO in order to enhance the performance of the distillation unit.

**Table 4.4** Range of various instruments with their accuracy

| S. No. | Instruments | Accuracy | Range |
|---|---|---|---|
| **1** | **Solar power meter** | 10 $W/m^2$ | 0 - 1999 $W/m^2$ |
| **2** | **Thermocouple (PT-100)** | ± 1°C | -50 - 110°C |
| **3** | **Measuring cylinder** | ± 10 ml | 0-2000 ml |
| **4** | **Anemometer** | 1-4 | 0.4-30 m/s |
| **5** | **Hygrometer (Ambient temperature)** | ± 1°C | -50 - 70°C |

**Table 4.5** The maximum uncertainties for the evaluated parameters

| Parameters | Uncertainty (%) |
|---|---|
| $h_{cwg}$ | 2.1 |
| $h_{rwg}$ | 3.4 |
| $h_{ewg}$ | 1.8 |
| $h_{twg}$ | 2.3 |
| $h_{lw}$ | 3.3 |

The cylinders have been made from copper due to their longer durability, better thermal conductivity with being noncorrosive and non-toxic. In the present study, a commercial-grade paraffin wax and copper oxide (nanoparticles) have been used, as shown in Fig. 4.3. The thermal conductivity of the PCM and NPCM have been measured using Hot Disk TPS 500 Thermal conductivity analyzer (manufactured in Sweden) with measuring range from 0.02 to 100 W/m-K and an accuracy of 99%. The thermal conductivity of PCM and NPCM have been found to be 0.25 and 0.340 W/m-K, respectively. In each case, all six copper cylinders have been filled with 1.3 kg of PCM or NPCM (nanoparticle being 1% of PCM weight), and the blending of nanoparticle has been done on magnetic stir operating on a hot plate. The variation of relative humidity (RH) throughout the experimental runs have been monitored using a digital thermo hygrometer (HTC 103-CTH, Mumbai, India).

### 4.2.2 Operating principle

As illustrated from Fig. 4.1 that the solar radiation during the charging phase has been mostly transmitted through the glass cover and water basin, eventually being absorbed by the basin liner, which resulted into rising in temperature of basin liner. The basin liner transmits the absorbed thermal energy during the sunshine hours through the convection mode to the basin water, as depicted in Fig. 4.1.

The study aims to find a well-productive, reasonable and locally available solar distillation system. However, it is essential to know the role and the physics of heat transfer mechanism along with energy storage and decreasing thermal losses in solar still to attain optimum productivity. In the present study, paraffin wax (Phase change material (PCM)) has been used to store solar energy in the form of latent heat and sensible heat during the charging mode. The stored solar energy in PCM helps in maintaining the required temperature of water basin for longer duration necessary for obtaining continuous distillate output which is full filled by PCM during its discharging mode. However, with charging and discharging mode of PCM also

accompanies thermal loses which happens mainly through the glass cover and it depends heavily on the rate and the duration of charging and discharging of PCM. On the other hand, the rate and the duration of charging and discharging of PCM solely depends on the thermal conductivity of the PCM and hence, increasing its thermal conductivity increases the rate of charging and discharging accompanied with decrease in its charging-discharging duration. The introduction of CuO nanoparticles in paraffin wax increased its thermal conductivity approximately by 36% leading to an appreciable enhancement in the rate of charging as well as discharging. Further to increase the heat transfer rate between PCM and water basin copper cylinders have been used for the storage of paraffin wax (PCM).

All six copper cylinders during the charging mode have been heated mostly by convective heat transfer from the water basin and partially by the exposed surface to the incident solar radiation. The thermal energy from the copper cylinder has been transferred to PCM or NPCM due to conductive mode in the form of sensible heat till the melting of PCM or NPCM started. Once the PCM or NPCM started melting, the thermal energy in the form of latent heat has been stored, and at this point, the temperature of paraffin wax remains constant until complete melting occurred. After the complete melting, the temperature of PCM or NPCM again started to rise and stored energy in the form of sensible heat. During the sunset hours, the discharging mode starts with the cooling of PCM or NPCM and releasing their thermal energy, which has been transferred to the water basin through copper cylinder as a latent and sensible heat until equilibrium for temperature has been achieved.

## 4.3 Energy balance and heat transfer

Heat transfer in solar distillation depends mainly on energy transfer between the basin water, basin liner, transparent glass cover, PCM and, its storage materials. Transparent glass cover witnesses heat loss in the form of evaporative ($h_{ewg}$), radiative ($h_{rwg}$), and convective ($h_{cwg}$) heat transfer coefficient, and these heat transfer coefficient and losses have been computed using

Dunkle (Dunkle, 1961) correlations. During the consideration of energy balance equations and heat transfer mechanisms for solar still in all cases (SSS, SSPCM, and SSNPCM), some assumptions have been considered. These are the following:

1. The passive solar still system with single slope is considered leak-proof with proper insulation, and side losses are neglected.
2. The heat capacity has been insignificant for glass cover, storage copper cylinder, basin liner, and insulating material in comparison to PCM or NPCM and basin water.
3. Heat transfer between copper cylinder and PCM or NPCM has been principally due to conduction with convection mode being negligible.
4. Heat transfer has been neglected between the copper cylinder and basin liner, and copper cylinder and glass cover.
5. In the present study, the thermal gradient throughout the PCM or NPCM has been not considered, and the simplicity in average calculation temperature has been quoted.

### 4.3.1 Heat transfer between water basin and glass cover

In the present study, for all three cases, heat transfer between the glass cover and water basin occurred predominantly due to convective, evaporative, and radiative mode. The convective mode depends mainly on flow characteristics, heat conduction, and fluid properties. The convective heat transfer between the glass cover and water basin surface occurred through the humid air and existed because of the temperature difference between them. Inside the solar still, the convective rate of heat transfer can be determined using Eq. (4.1):

$$Q_{Cwg} = h_{Cwg} \times \left(T_w - T_{gi}\right) \quad (4.1)$$

,where $h_{cwg}$ has been calculated using Dunkle (Dunkle, 1961) correlations.

Heat transfer due to radiative mode includes emission of internal energy by the object and glass cover inclination with respect to water basin has been small enough to consider the view factor

as unity. The radiative heat transfer rate between the glass cover surface, and water can be calculated using Eq. (4.2) and, $h_{rwg}$ has been calculated using Eq. (4.3) (Chen et al., 2013; Dunkle, 1961).

$$Q_{rwg} = h_{rwg} \times \left(T_w - T_{gi}\right) \tag{4.2}$$

$$h_{rwg} = \varepsilon_{eff}\sigma\left[(T_w + 273)^2 + \left(T_{gi} + 273\right)^2\right]\left(T_w + T_{gi} + 546\right) \tag{4.3}$$

The effective emissivity existing between water mass and glass cover can be determined using Eq. (4.4) (Sharshir et al., 2017).

$$\varepsilon_{eff} = \left(\frac{1}{\varepsilon_w} + \frac{1}{\varepsilon_g} - 1\right)^{-1} \tag{4.4}$$

At a given temperature inside the solar still evaporation occurs when the water vapor pressure becomes lower to its saturation pressure. The mechanism of radiative heat transfer can be explained through the evaporative mode of heat transfer. The rate of evaporative mode of heat transfer depends greatly on the relative humidity and air-water temperature difference, which can be considered as the participating media for the mechanism of radiative heat transfer in our proposed novel solar still. Fujita et al. (Fujita et al., 2010) mentioned in their study that as the relative humidity increases, the temperature of the water droplets decreases, whereas for higher relative humidity it increases. In evaporative heat transfer mode, an increase of the basin water temperature increases the evaporation energies which results higher distillate output. However, other metrological variables such as wind speed, dry bulb and wet bulb temperature as well as air density are not playing significant role in the mechanism of evaporative heat transfer and hence, these can be considered as non-participating media. The evaporative mode of heat transfer occurs between the water liquid-vapor interfaces (Chen et al., 2013; Dunkle, 1961) and can be expressed as in Eq. (4.5):

$$Q_{ewg} = h_{ewg} \times (T_w - T_{gi}) \tag{4.5}$$

,where $h_{ewg}$ has been calculated by using Dunkle (Dunkle, 1961) correlation as given in Eq. (4.6):

$$h_{ewg} = 13.273 \times 10^{-3} \times h_{Cwg} \times \left[\frac{P_w - P_{gi}}{T_w - T_{gi}}\right] \quad (4.6)$$

The values of $P_w$ and $P_{gi}$ have been calculated using Eq. (4.7) and (4.8), respectively, as given by Fernandez et al.(Fernández and Chargoy, 1990).

$$P_w = exp^{\left(25.317 - \frac{5144}{T_w + 273}\right)} \quad (4.7)$$

$$P_{gi} = exp^{\left(25.317 - \frac{5144}{T_g + 273}\right)} \quad (4.8)$$

The total heat transfer rate between the water basin and glass cover for all the three cases can be calculated using Eq. (4.9) and (4.10):

$$Q_{twg} = Q_{cwg} + Q_{rwg} + Q_{ewg} \quad (4.9)$$

$$Q_{twg} = h_{twg} \times (T_w - T_{gi}) \quad (4.10)$$

,where $h_{twg}$ has been calculated using Eq. (4.11):

$$h_{twg} = h_{cwg} + h_{rwg} + h_{ewg} \quad (4.11)$$

The energy balance equation occurring between the liner and water basin can be expressed by Eq. (4.12)

$$I\tau_g\tau_w\alpha_l = h_{lw}(T_l - T_w) \quad (4.12)$$

## 4.4 Uncertainty analysis

Eq. 4.13 represents the equation developed by Kline and McClintock(Kline and McClintock, 1953) for calculating the uncertainties on the basis of accuracies of mirrored parameters and properties involved while evaluating the parameters (Y).

$$\frac{\delta Y}{Y} = \sqrt{\left\{\frac{\delta X_1}{X_1}\right\}^2 + \left\{\frac{\delta X_2}{X_2}\right\}^2 + - - - - - + \left\{\frac{\delta X_n}{X_n}\right\}^2} \quad (4.13)$$

Where Y denotes the evaluated parameters such as $h_{cwg}$, $h_{rwg}$, $h_{ewg}$, $h_{twg}$ and $h_{lw}$, and X denotes the measured parameters like temperature, solar intensity and mass. The maximum uncertainty for the evaluated parameters have been listed in Table 4.5.

## 4.5 Results and discussion

### 4.5.1 Hourly variation of ambient, glass cover temperature, and solar intensity

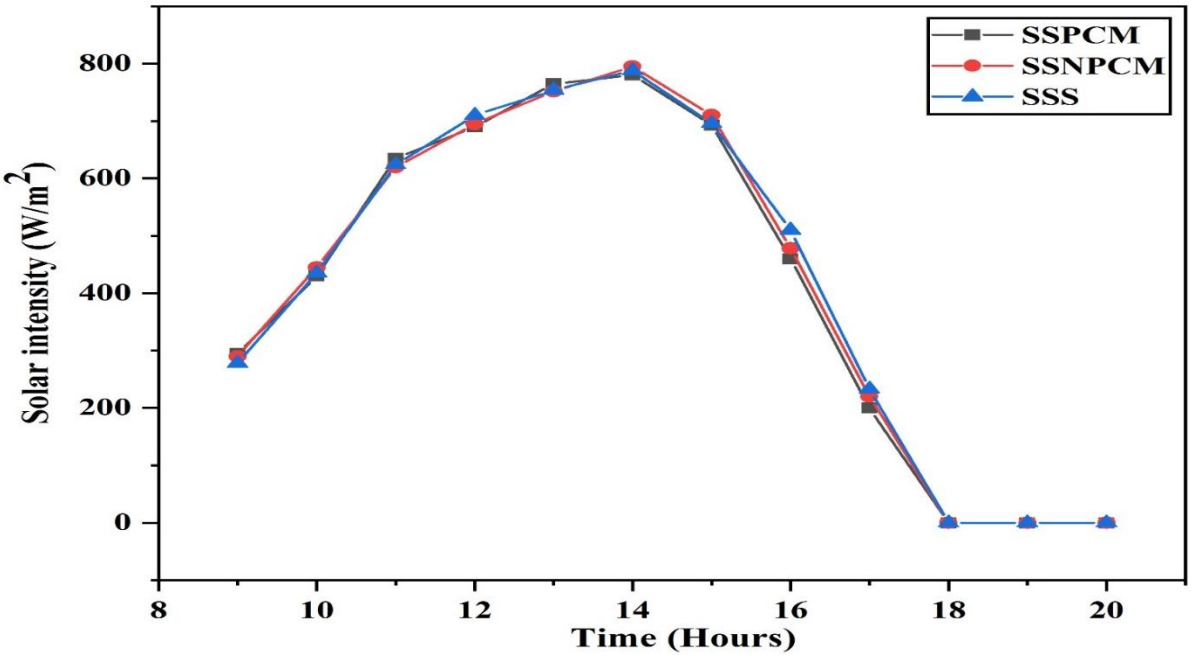


**Fig. 4.4 (a)** Solar intensity variation with respect to time

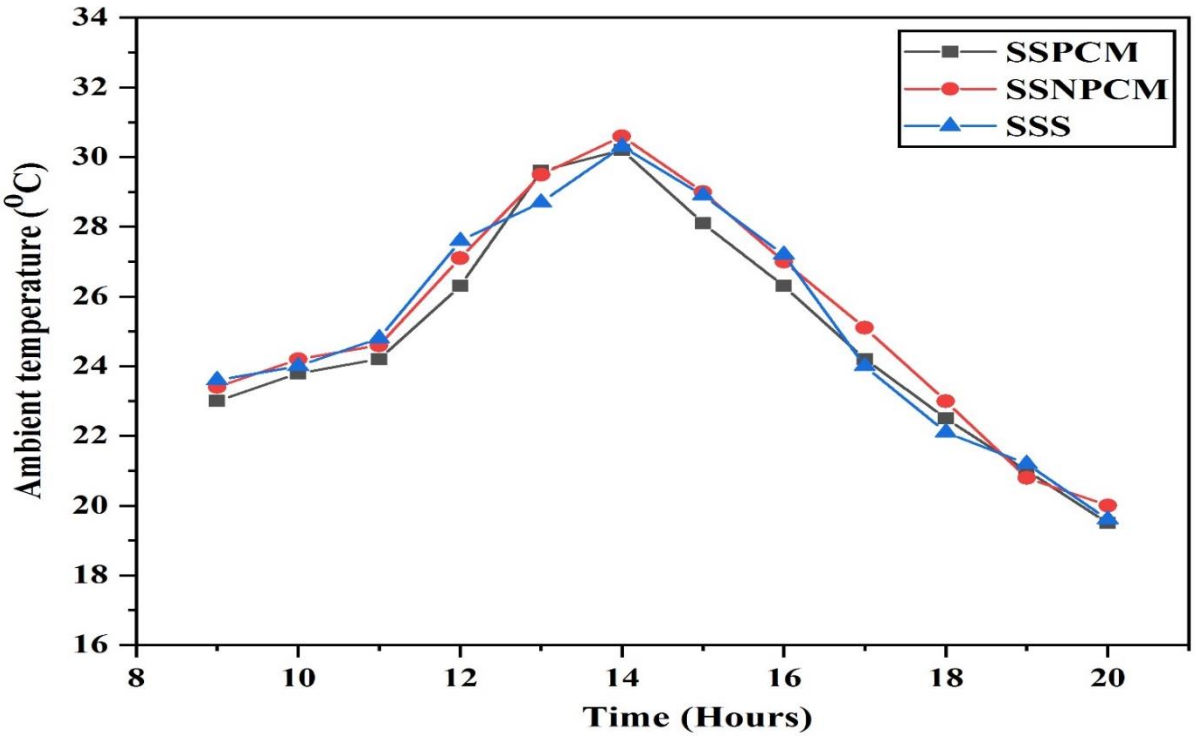


**Fig. 4.4 (b)** Ambient temperature variation with respect to time

In this section, the results relating to the performance of SSS, SSPCM, and SSNPCM have been compared for Varanasi city (25.3176° N, 82.9739° E), Uttar Pradesh, India. During the October month, the solar intensity is lower as compared to the summer. Figs. 4.4 (a) and 4.4 (b) show the hourly variation of solar intensity and ambient temperature in all three conditions. Fig. 4.4 (a) reveals that solar radiation in India is very high (795 W/m$^2$) even in the month of October, which is considered as the starting of the winter season. Even though for all three cases, the experiments have been performed on three different days, the variation in solar intensity and ambient temperature have been nominal, suggesting that the performance of the solar still would not have been interfered due to minor variations of meteorological parameters.

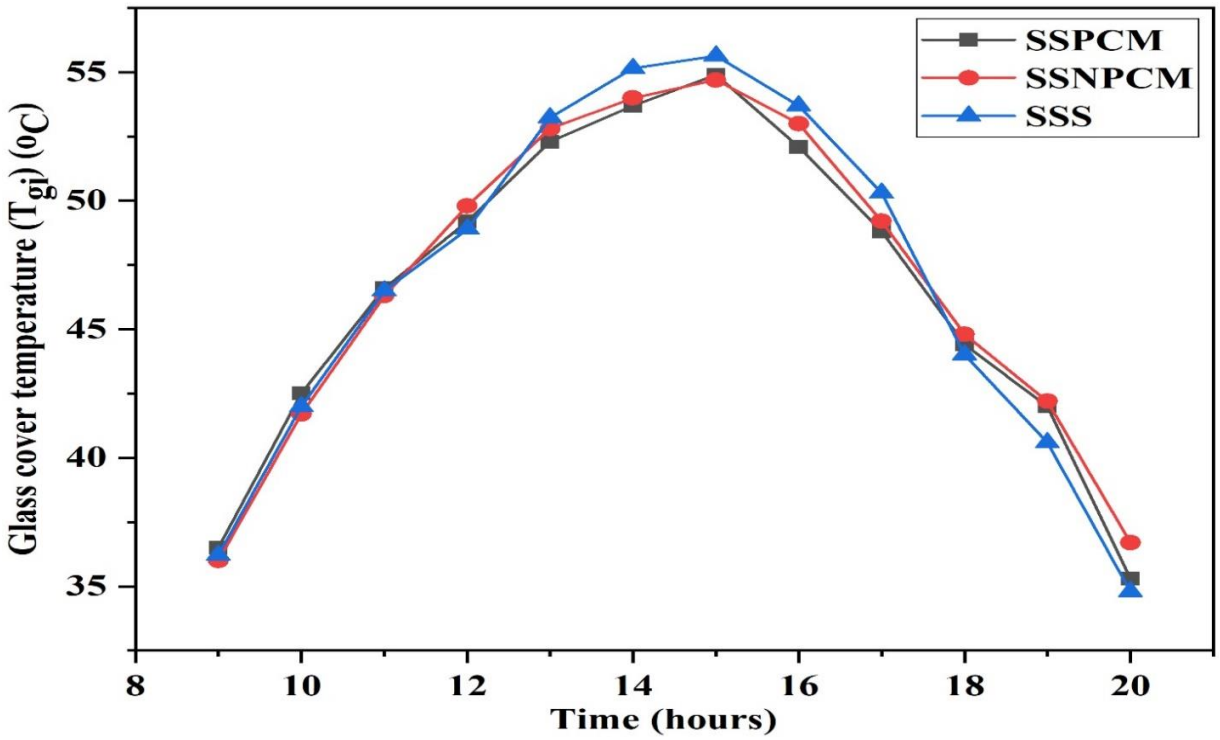


**Fig. 4.5** Hourly variation of glass cover temperature

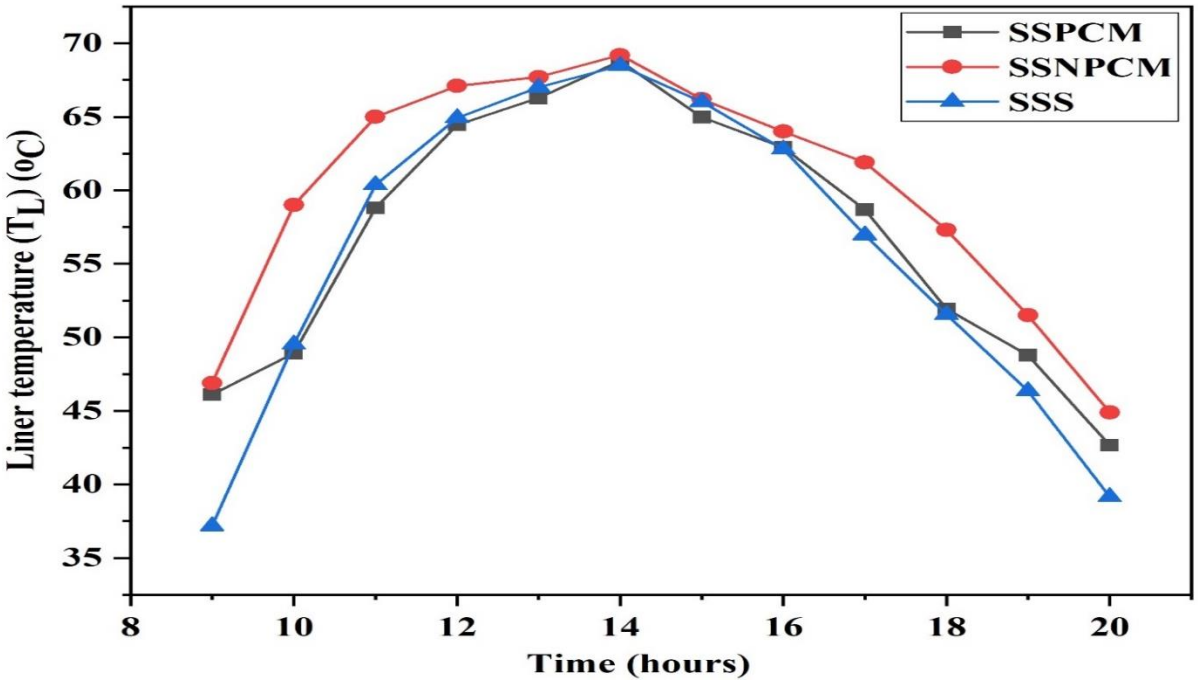


**Fig. 4.6** Hourly variation of liner temperature

Fig. 4.5 represents the hourly variation of glass cover temperature for SSS, SSPCM, and SSNPCM. It is observed that the variation of glass cover temperature for three conditions has been the same and close to each other as compared to that of the water basin and liner

temperature. The similar glass cover temperature for all three conditions have been due to high transmittance (90%) and lower absorptivity (5%) of glass. The temperature of glass increased with time and reached the highest temperature during 1.00 – 2.00 PM. It can also be considered that the temperature of the inner glass has been close to the temperature of the water during the early hours of the day. However, as the time of sunshine increases, the difference between glass and water widens due to water absorbing some of the incident solar radiation and also, receives heat from the liner, while the transparent glass cover transmits maximum incident solar radiation.

### 4.5.2 Hourly variation of liner temperature, basin water, PCM, and NPCM

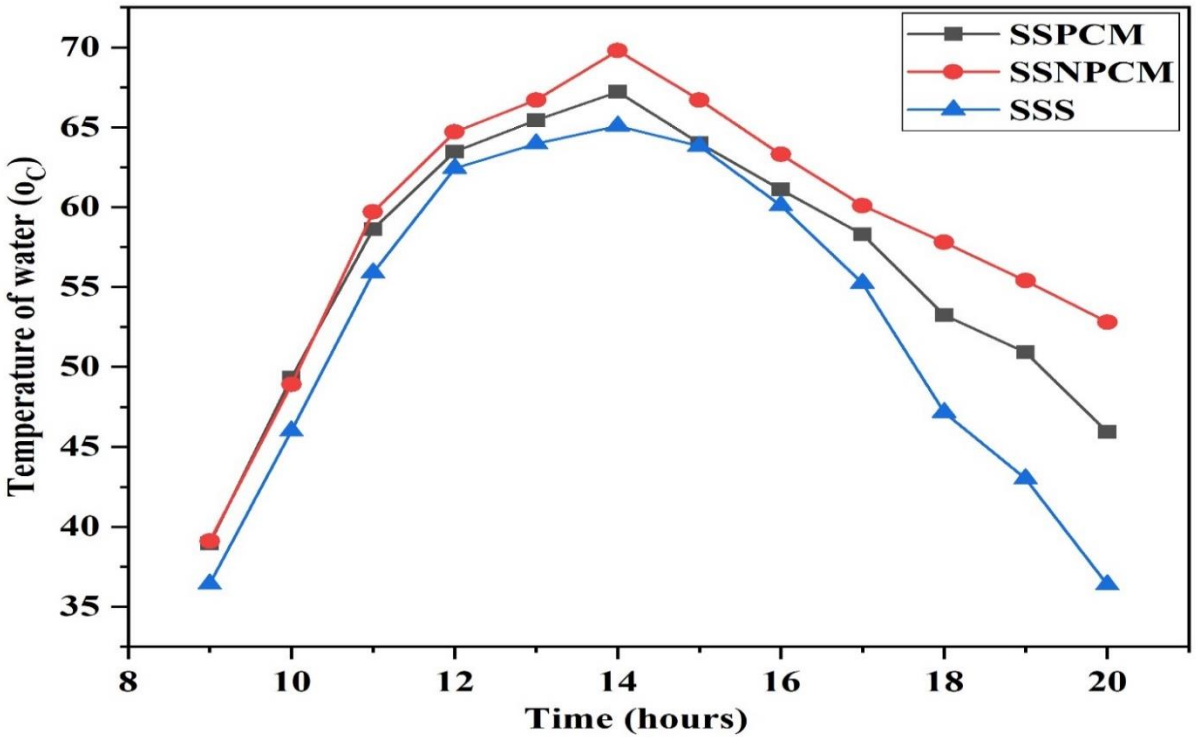


**Fig. 4.7** Hourly variation of water basin temperature

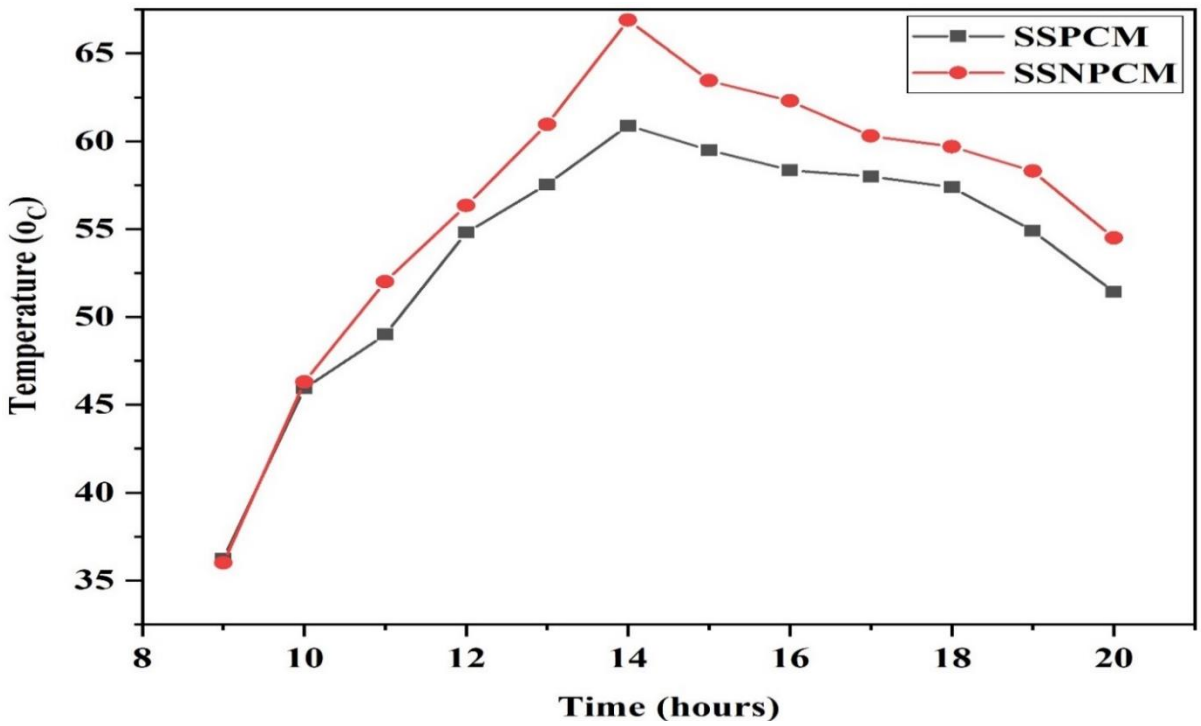


**Fig. 4.8** Hourly variation of PCM and NPCM temperature

Fig. 4.6 represents the hourly variation of liner temperature. The basin has been colored black so that it can absorb most of the incident radiation, and can transfer thermal energy quickly to the water basin. It has been observed that basin liner temperature, water temperature, glass temperature and PCM temperature follow the same solar radiation intensity profile. As the solar radiation intensity increases with time, the rate of heat transfer increases due to convection from basin liner to water basin and further solar energy is stored in PCM. However, the temperature of the basin liner and the other elements of the solar still decrease faster with time due to decrease in ambient temperature. The maximum liner temperature for SSS, SSPCM, and SSNPCM have been recorded around 2 pm with values being 68.47, 68.39, and 69.2 $^{o}$C, respectively. It can be observed that liner temperature quickly reaches a maximum and also loses its temperature quickly after 2 pm because the liner has low thermal storage ability and transfers heat energy to water present in the basin.

Fig. 4.7 manifest the hourly variation of water basin temperature and, it can be observed that the maximum temperature has been recorded at 2 pm. The maximum temperature attained by

SSNPCM (69.8 $^{o}$C) has been much higher as compare to SSS (65.07 $^{o}$C) and SSPCM (67.2 $^{o}$C), which resulted in the higher distillate. In most of the operational hours, the water basin temperature of SSNPCM has been higher as compared to SSPCM and SSS due to the addition of nanoparticle, which increased the charging and discharging capacity of the system. The increase in the charging and discharging capacity of SSNPCM has been due to a significant increase in the thermal conductivity of the storage material.

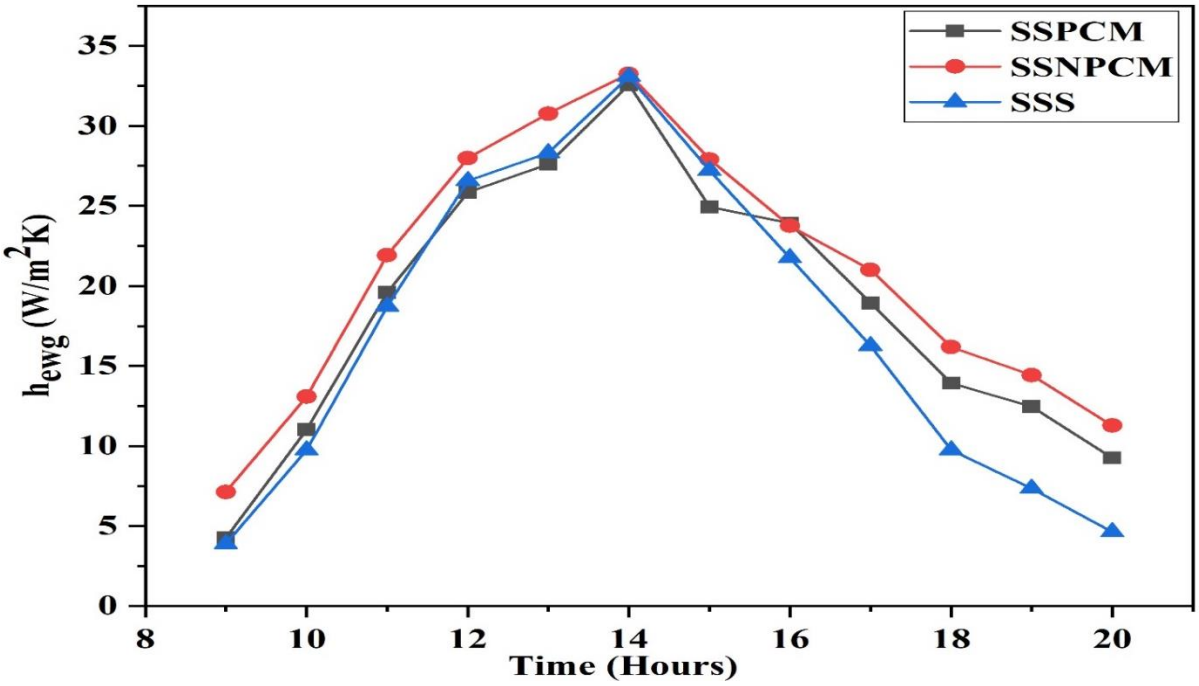


**Fig. 4.9** Hourly variation of evaporative heat transfer coefficient

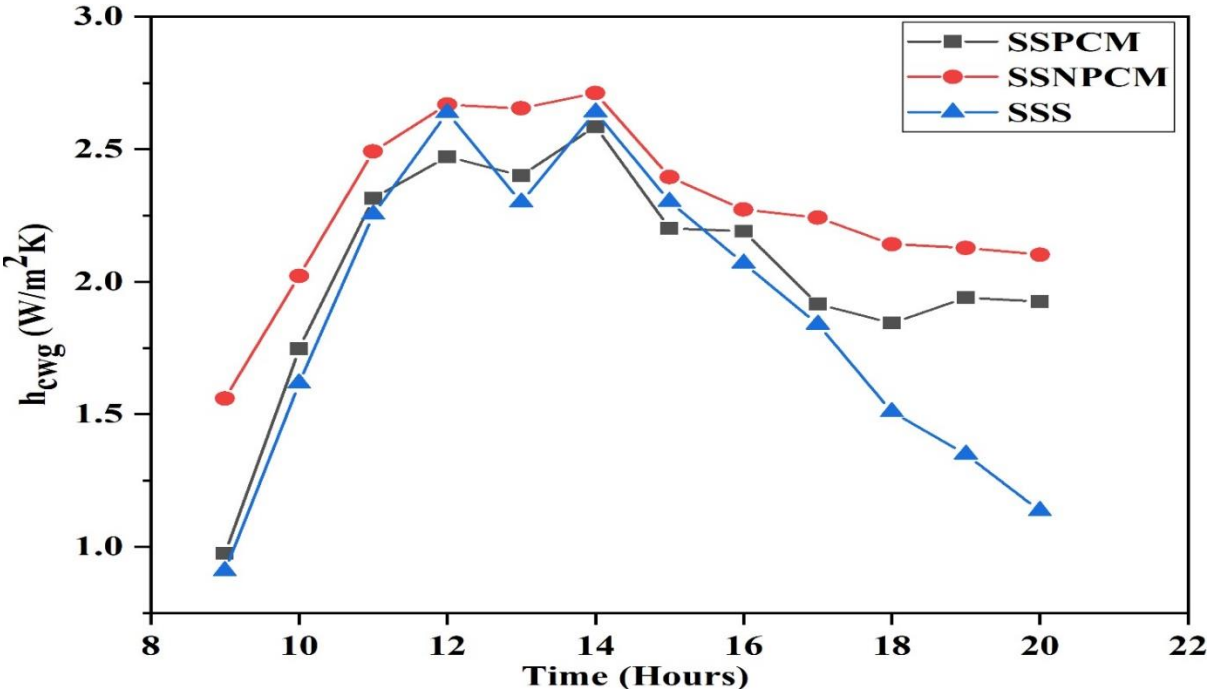


**Fig. 4.10** Hourly variation of convective heat transfer coefficient

Fig. 4.8 represents the hourly variation of PCM and NPCM. The PCM temperature for both cases (SSPCM and SSNPCM) during the charging mode has been lower as compared to water basin temperature and stores thermal energy to be utilized in the discharging phase to increase or maintain the water basin temperature. It can be noted that the temperature of PCM or NPCM increases with time as the solar intensity increases.

During the charging mode, firstly, the thermal energy has been stored as a sensible heat for SSPCM or SSNPCM until PCM or NPCM reaches its melting point. After which the temperature of PCM or NPCM remains constant for a small duration until it witnesses phase transformation. Once phase transformation gets completed, the $T_{PCM}$ and $T_{NPCM}$ increases again because of sensible heat stored in liquid PCM and reaches the maximum temperature. The maximum temperature attained by PCM and NPCM has been 60.89 $^{o}$C and 66.91 $^{o}$C, respectively. The significant increase in temperature of NPCM as compared to PCM declares the effect of nanoparticles added with paraffin wax. In the absence or low radiation discharging mode of the SSPCM and SSNPCM started where the thermal energy stored in PCM or NPCM has been released due to a reduction in temperature. Firstly the sensible heat has been released

until the temperature of PCM and NPCM reaches its solidification point, where the temperature of PCM or NPCM remains constant throughout the hardening process and then releases energy in the form of the latent heat which has been stored during the charging phase. Dsilva et al. (Chaichan and Kazem, 2018; Dsilva Winfred Rufuss et al., 2018) also mentioned in their study that doping of nanoparticle into PCM increased the temperature of PCM and basin water which resulted into higher daily productivity.

### 4.5.3 Variation of heat transfer coefficient for SSS, SSPCM, and SSNPCM

In Figs. 4.9-4.13 indicates the hourly variation of heat transfer coefficients ($h_{ewg}$, $h_t$, $h_{rwg}$, $h_{cwg,}$ and $h_{lw}$) associated with the solar distillation units. In the present study, the calculation of the heat transfer coefficients associated with water and glass cover is necessary because maximum heat loss occurs between these two components during charging and discharging mode.

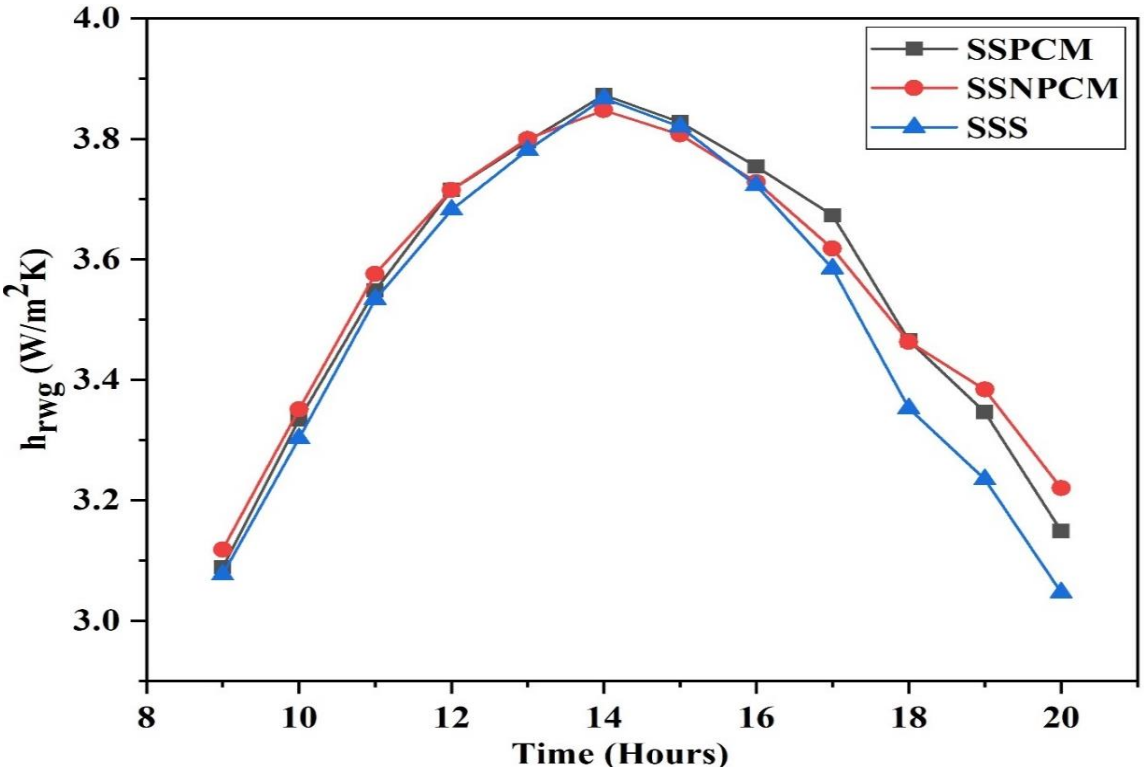


**Fig. 4.11** Hourly variation of radiative heat transfer coefficient

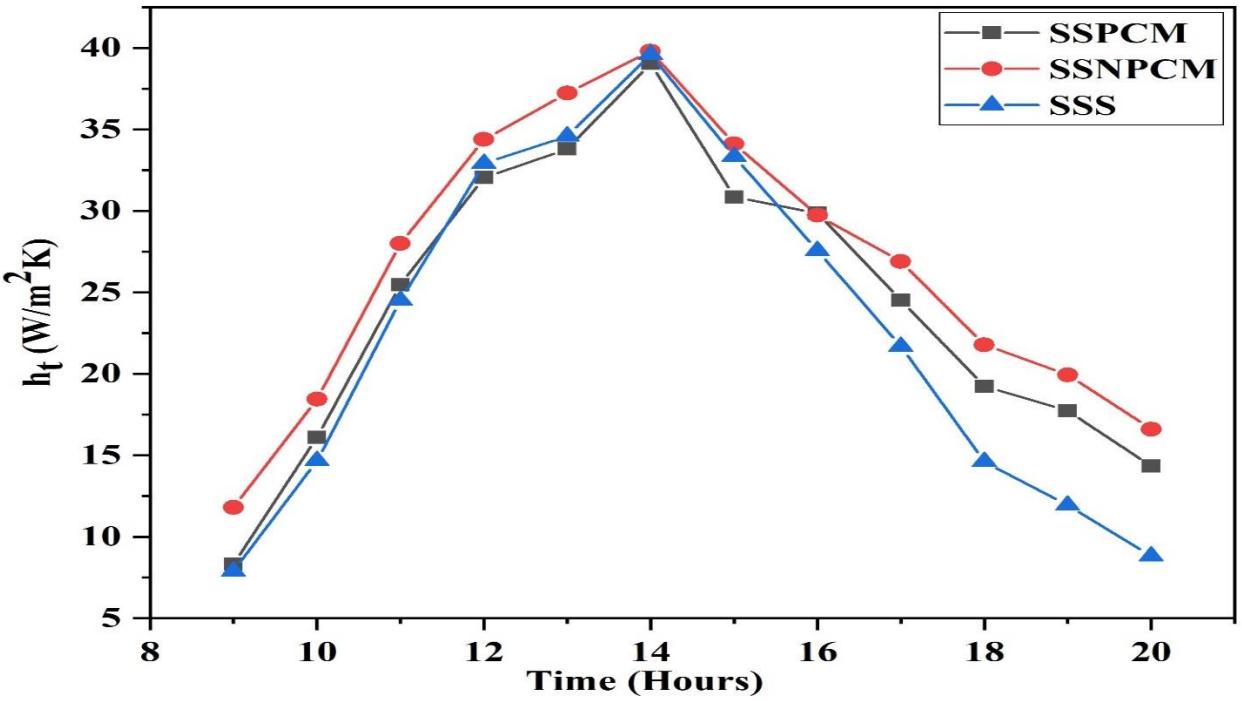


**Fig. 4.12** Hourly variation of total heat transfer coefficient

In the observed period, the evaporative heat transfer coefficient plays a major role in total heat transfer between the water basin and glass cover as compared to radiative and conductive heat transfer coefficients. The maximum value for $h_{ewg}$ (SSNPCM=33.25, SSPCM=32.57, and SSS=33.08 W/m$^2$-K), $h_{rwg}$ (SSNPCM=3.85, SSPCM=3.80, and SSS=3.86 W/m$^2$-K), $h_{cwg}$ (SSNPCM=2.7, SSPCM=2.5, and SSS=2.65 W/m$^2$-K), $h_t$ (SSPCM=39.80, SSPCM=39.03, and SSS=39.58 W/m$^2$-K) have been observed around 2 pm when the maximum temperature has been achieved by the water basin. The substantial-high values for the heat transfer coefficient associated with evaporative mode as compared to radiative and convective mode confirm the high rate of evaporation, resulting in distillate output. The variation of relative humidity has been in the range of 44 ± 9 % for all three experimental runs. The rate evaporative mode of heat transfer depends greatly on the relative humidity and air-water temperature difference. Fujiita et al. (Fujita et al., 2010) in their study mentioned that as the relative humidity increases, the temperature of the water droplets decreases, whereas for higher relative humidity it

increases. In evaporative mode of heat transfer, an increase in basin water temperature enhances the evaporation energy which results higher distillation output.

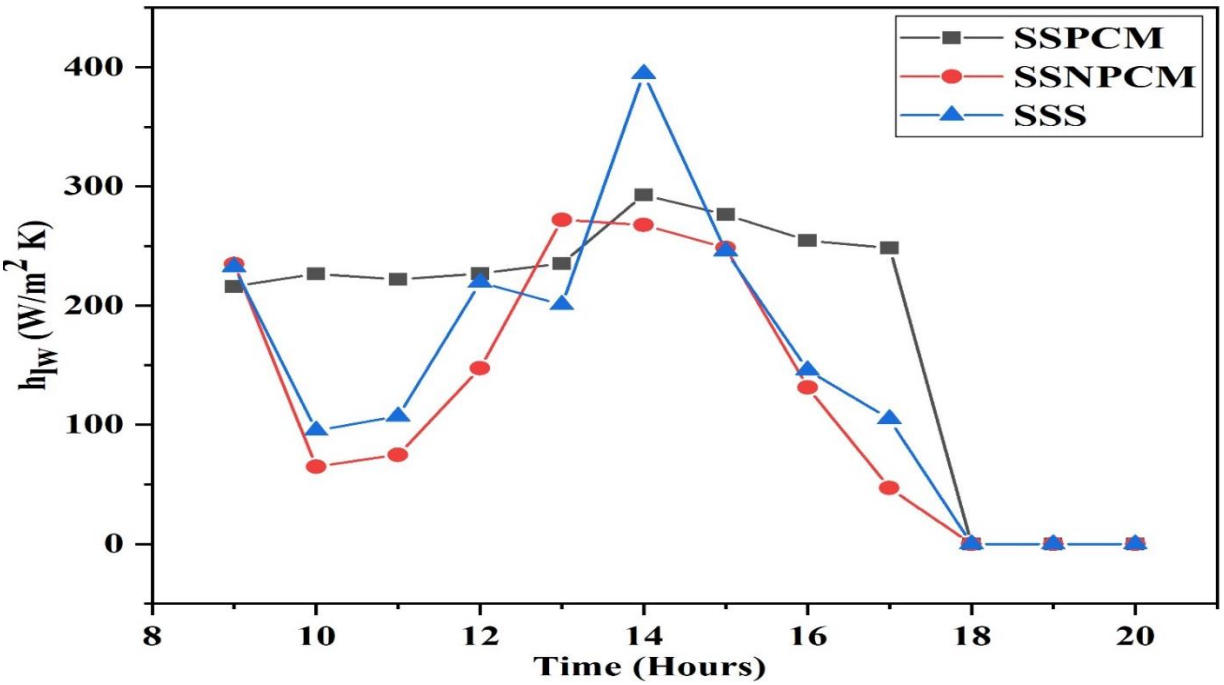


**Fig. 4.13** Hourly variation of heat transfer coefficient between water and liner

It can also be observed from Fig 4.9-4.12 that for all three conditions (SSS, SSPCM, and SSNPCM), the heat transfer coefficients associated between the water basin and glass cover have similar trend with values being in the same range, and this also confirms that nanoparticle had a nominal effect on these heat transfer coefficients. El Sebaii et al. (El-Sebaii et al., 2008) also calculated the heat transfer coefficients associated with the solar still coupled with PCM, where the maximum value for the evaporative heat transfer coefficient was approximately equal to 36 W/m$^2$-K and followed the similar trend as observed in the present study. Shukla et al. (Shukla and Sorayan, 2005) and Tiwari et al. (Tiwari et al., 1994) also calculated the heat transfer coefficients associated with solar still where evaporative heat transfer was the dominating factor as compared to convective and radiative heat transfer. Even though the nanoparticle had nominal or no effect on evaporative, conductive, and radiative heat transfer coefficients, the increased basin water temperature of SSNPCM as observed in Fig.4.7

compared to other two conditions confirm that total heat transfer increased which resulted into higher energy storage in the form of sensible and latent heat from in paraffin wax.

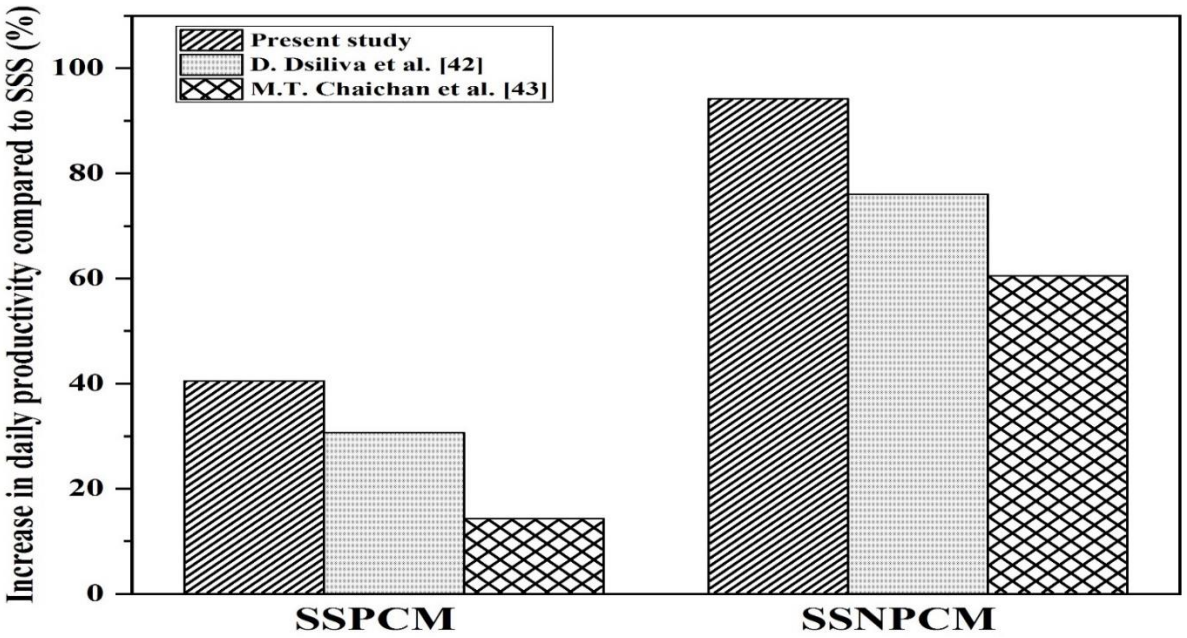


**Fig. 4.14** Comparison of increased daily productivity as compared to SSS

In Fig. 4.13 no proper trend has been observed for the heat transfer coefficient ($h_{lw}$) present between the liner and water basin in all three conditions. However, after sunset, as the temperature of the water basin and liner becomes nearly equal, the value of heat transfer coefficient ($h_{lw}$) nears to zero. Sebaii et al.(El-Sebaii, 2000; El-Sebaii et al., 2009a; El-Sebaii et al., 2008; El-Sebaii et al., 2009b) in there various studies mentioned similar values for heat transfer coefficients present between liner and basin water.

### 4.5.4 Effect of PCM, nanoparticle and copper cylinder on daily productivity

The total daily distillate of SSS, SSPCM, and SSNPCM have been 1980, 2782, and 3845 ml/$m^2$-day. The total distillate for SSPCM increased significantly due to the introduction of PCM, which led to distillation continue even in the absence of solar radiation, while in the case of SSNPCM, the system witnessed much higher output due to increased heat transfer rate by introducing nanoparticle in PCM.

Fig. 4.14 represents the increased daily productivity as compared to SSS, and these results have been compared and validated with different two similar studies reported by Dsilva et al. (Dsilva Winfred Rufuss et al., 2018) and Chaichan et al. (Chaichan and Kazem, 2018). It can be observed that the daily productivity for SSPCM in the present study increased by 40.5 % while for Dsilva et al. (Dsilva Winfred Rufuss et al., 2018) and Chaichan et al. (Chaichan and Kazem, 2018) it increased by 30.66 and 14.28 %, our experimental setup showed better results due to the storage of PCM in the copper cylinder which enhanced the heat transfer rate resulting in more productivity. Similar results have been also observed by Arunkumar et al. (Arunkumar et al., 2013) , where daily productivity increased significantly from 3520 to 4460 ml/$m^2$-day when PCM stored in the copper spherical balls were introduced compared to solar still coupled with a solar concentrator. In the present study, a significant increase in daily productivity has been observed when nanoparticle (CuO) has been introduced into PCM stored in a copper cylinder. In Fig. 4.14, where, Dsilva et al. (Dsilva Winfred Rufuss et al., 2018) and Chaichan et al. (Chaichan and Kazem, 2018) reported a 76 and 60.51 % increase in daily productivity for SSNPCM while the present study observed 94.16 % increase. This better performance has been because copper has better thermal properties as compared to other materials such as aluminium or stainless still, which enhanced the heat transfer rate.

## 4.6 Summary

Thermal energy storage (paraffin wax) doped with nanoparticles (CuO) stored in a copper cylinder showed substantial improvement in daily productivity. The maximum and average temperature of the water basin has been highest for SSNPCM followed by SSPCM, and SSS. The present study revealed that the evaporative, convective, and radiative heat transfer coefficients increase with an increase in solar intensity. The combination of paraffin wax and nanoparticles increase its thermal conductivity resulting a better heat transfer rate.

Cylindrical copper storage showed better performance as compared to spherical copper storage used for PCM or NPCM, and this improved performance has been due to increased surface area for a given volume. Charging and discharging time for NPCM have been decreased compared to PCM due to their improved thermal conductivity.